Design Considerations for a Space-based Transit Search for Earth Analogs

by

Thomas Gavin Beatty

B.A., Harvard University (2006)

Submitted to the Department of Physics
in partial fulfillment of the requirements for the degree of

Master of Science in Physics

at the

MASSACHUSETTS INSTITUTE OF TECHNOLOGY

June 2009

Author .....
Department of Physics
May 26, 2009

Certified by .....
Professor Sara Seager
Associate Professor
Thesis Supervisor

Accepted by .....
Professor Thomas Greytak
Associate Department Head for Education

Design Considerations for a Space-based Transit Search for Earth Analogs

by

Thomas Gavin Beatty

Submitted to the Department of Physics
on May 26, 2009, in partial fulfillment of the
requirements for the degree of
Master of Science in Physics

Abstract

An extrasolar planet discovered around one of the brightest stars in the sky would be a prime target for follow-on observing and characterization, especially if the planet were within the star's habitable-zone. The brightest stars are, however, often not considered to be practical targets for photometric planetary transit searches, despite the scientific rewards that finding a planet around these stars would provide. ExoPlanetSat is a proposed satellite constellation that will survey the brightest G- and K-dwarfs across the entire sky and look for transits of Earth-sized planets in the habitable-zone. By using measurements of stellar orientations provided primarily by asteroseismic observations, only those stars whose axes lie near 90° to our line of sight will be observed. This increases the transit probability of a habitable-zone planet from 0.5% to 5%, lowering the number of stars that need to be examined by a factor of ten. This in turn enables the design of a practical survey of the brightest stars. A proposed concept of operations envisions thirty small spacecraft in low Earth-orbit, each individually targeted onto a bright star. Over the course of four years, these spacecraft will able to observe a sufficient number of solar-like stars to expect the detection of three habitable-zone Earths with high statistical confidence, assuming that every star has such a planet in orbit.

Thesis Supervisor: Professor Sara Seager
Title: Associate Professor

Acknowledgments

Firstly, I am grateful to my thesis adviser, Sara Seager, for her guidance and encouragement — especially in the final stages of writing. Josh Winn also provided invaluable comments on the draft of this thesis, besides answering question that I had during writing. George Ricker generously discussed many aspects of the optical design of the spacecraft. I would also like to thank Elizabeth Wood and my Riverside, CT based consulting team.

Biographical Note

Thomas Beatty is a graduate of Phillips Exeter Academy and of Harvard University, where he received a Bachelor of Arts with Honors in Astronomy and Astrophysics and was awarded the Thomas T. Hoopes Prize. He was a recipient of the Whiteman Fellowship at MIT, and will be a Distinguished University Fellow at the Ohio State University.

Contents

List of Figures

List of Tables

1. Introduction

In the decade since the discovery of the first transiting planet in orbit around HD 209458 (Charbonneau et al. 2000; Henry et al. 2000), the study of extrasolar planets has grown by leaps and bounds. No longer dependent on just the traces of a radial velocity orbit, it is now we are beginning to place constraints on the atmospheres, internal structures, and even the wind patterns of planets orbiting other stars. In conjunction with the growing understanding (and number) of transiting Hot Jupiters, the field has begun to shift away from the discovery of these massive planets, and towards the discovery of even smaller, Earth-like, worlds.

There has been a corresponding shift in the design of transit surveys. The first transit surveys - such as TrES (Alonso et al. 2004), HAT (Bakos et al. 2004), XO (McCullough et al. 2005), and SuperWASP (Street et al. 2003) - are all ground-based surveys that are primarily sensitive to Jupiter-sized planets. These surveys also target dim stars near $m_v = 11$, so that they can have sufficient stars in each field of view to statistically expect a transit detection. It is also difficult for these surveys to probe for planets in orbital periods longer than a month, since the duty cycle of the surveys and the movement of the Sun restrict the continuous time that a star may be monitored. Some surveys, such as MEarth (Nutzman & Charbonneau 2008), have pushed towards smaller planet radii by targeting M-dwarfs, but it will be very difficult to detect an Earth-sized planet orbiting a Sun-like star — particularly one in the habitable-zone — with one of these ground-based surveys in the foreseeable future.

What are needed for the detection of an Earth-like planet in the habitable-zone are spaced-based photometric surveys. It is possible to achieve the required photometric precision and accuracy to detect Earth-like planets around M-dwarfs from the ground (e.g. MEarth), but and the order of magnitude difference in transit depth of an Earth in

front of a Sun-like star (530ppm vs. 84ppm) mean that ground-based surveys for Earths around solar-like stars are impractical due to atmospheric effects. Unfortunately, the low-transit probabilities for habitable-zone Earths make any such planet-hunting spacecraft a major endeavor, since it must take precise photometry on tens of thousands of stars simultaneously. Indeed, the Kepler spacecraft will target over 100,000 stars in its field of view. A necessary result of needing this many stars is that all of the targets are fairly dim, on the order of $m_V = 12$, so that all of the stars may fit into the Kepler's field of view. Finding Earth-like planets around brighter stars would be preferable, but imaging 100,000 brighter stars would require a field of view impractically large.

One possible solution to the difficulty of targeting bright stars would be to launch several different telescopes into orbit, and have each observe a specific target. This would solve the field of view problem, but would have to surmount the low 0.5% transit probability of habitable-zone Earths. Assuming every star has an Earth in orbit within the habitable-zone, a survey would need to observe 200 stars to statistically expect a detection. To expect three detections, and thereby increase the statistical confidence in finding at least one planet, would require 600 stars. With individually targeted spacecraft, this would require either hundreds of spacecraft in orbit or hundreds of years of observing. Conducting such a survey would be impractical with individually targeted spacecraft.

However, if one could measure beforehand the orientation of the probable planetary systems, and then select those stars that were near 90° to our line of sight, the transit probability for this select group of stars would be greatly improved. A transit survey of the brightest stars would then only have to examine the stars with favorable orientations for transits, reducing the number of spacecraft needed from several hundred to several dozen.

Here, we describe the ExoPlanetSat constellation. ExoPlanetSat is a mission to survey the brightest G- and K-dwarfs in the sky for transiting habitable-zone Earths. Using

measurements of the stellar rotational orientation provided by either spectroscopic or asteroseismic measurements, ExoPlanetSat will choose target stars that are oriented at nearly 90° to our line of sight — enhancing the transit probability by an order of magnitude. Since the targets of the survey will bright, with $m_V \leq 7$, the required telescope diameter to detect a transit is relatively small: 15.1cm. Using a constellation of several differently sized telescopes on their own individual spacecraft, ExoPlanetSat would be able to survey all of the promising G- and K-dwarf transit candidates within four to five years. Using even smaller 8cm triple CubeSat-sized spacecraft will limit the survey to stars brighter than $m_V = 6$, which would allow for thirty of these small spacecraft to expect one detection of a habitable-zone Earth.

2. Targeting Bright Stars

The main problem facing a photometric transit survey of the brightest stars is the spread of the stars around the sky; they are so far apart that usually only one can be observed at a time. Coupled with the low transit probability of a planet within the habitable-zone (approximately 0.5%) and the amount of observing time needed to see a sufficient number of transits to confirm a detection (one to two years), this means that a survey of the bright stars would have either have to observe with hundreds of telescopes for a few years, or a few telescopes for hundreds of years. If, however, we can measure stellar orientations with respect to the plane of the sky, this math changes: only the stars oriented near 90° - which implies higher transit probabilities - would need to be observed. Depending upon the precision and accuracy of the measurement, this would lower the required number of stars from several hundred to several dozen.

We have therefore made a general derivation of how different measurements of the stellar orientation will affect the transit probability of a planetary system. We have also

considered specifically how measurements of stellar orientations can be made through rotational velocity measurements and asteroseismology. Finally, we have also examined the effect that inclination of the planetary system with respect to the stellar equator has on the transit probability.

2.1. General Transit Probabilities

In general, for calculating transit probabilities we will be interested in two quantities: the angle the parent star's equator makes with the plane of the sky, and the angle the planetary orbit makes with the stellar equator. These two angles allow us to determine the angle the planet's orbit makes with the plane of the sky, and whether or not the planet will transit. Conventionally, all three of these angles are denoted by the variable i. To reduce confusion, we will use i to refer to the angle that the planet's orbit makes with the plane of the sky, I for the angle that the stellar equator makes with the plane of the sky, and the variable ψ for the angle that the planet's orbit makes with the stellar equator.

With no prior information about the orientation of a planetary system, we must assume that the orientation is randomly and evenly distributed over all possible orientations. In this case, for circular orbits the probability that the system will show a planetary transit is R_*/a (Borucki & Summers 1984), where R_* is the radius of the parent star, and a is the semi-major axis of the orbit. This may be derived by first considering the angular momentum vector of the planetary orbit. Each possible orbital orientation possesses a distinct angular momentum vector. If the angular momentum of the orbit is the same for all orientations, then the magnitudes of each of the angular momentum vectors are the same, and the complete set of all the vectors describes a sphere in space, centered on the parent star.

On the surface of this imaginary sphere, the set of angular momentum vectors which correspond to transiting orbits are arranged in a band centered along the "equator" of the sphere. The plane of the equator coincides with the plane of the sky. The width of this band is given by the maximum orbital inclination that yields a transit, which is

$$\theta = \arcsin\left(\frac{R_*}{a}\right) \tag{1}$$

Now, it is possible to project the surface of this sphere onto a two-dimensional map; similar to a map of the Earth. Like a map of the Earth, it is useful to define a latitude (ϕ) and longitude (λ) on this map, which will have limits of $0 \leq \phi \leq 180°$ and $0 \leq \lambda \leq 360°$. In this projection, the band of transiting orbits is a strip of longitude, laying between the latitudes of $90° - \theta \leq \phi_{tr} \leq 90° + \theta$, where $\theta = \arcsin(R_*/a)$, as in equation (1).

The transit probability is then the fractional number of orbital orientations that lay inside this strip. In the case that no information is known about the orientation of the planetary system, all orientations are equally likely, and the probability density function (PDF) of the orientations is a uniform constant across the entire parameter map: $p(\phi, \lambda) = C$ (Figure 1). In this instance, the transit probability is then

$$\begin{aligned} P_{tr} &= \frac{\int_{90°-\theta}^{90°+\theta}\int_0^{360°} p(\phi,\lambda)R^2\sin(\phi)\ d\lambda\ d\phi}{\int_0^{180°}\int_0^{360°} p(\phi,\lambda)R^2\sin(\phi)\ d\lambda\ d\phi} = \frac{\int_{90°-\theta}^{90°+\theta}\int_0^{360°} C\ R^2\sin(\phi)\ d\lambda\ d\phi}{\int_0^{180°}\int_0^{360°} C\ R^2\sin(\phi)\ d\lambda\ d\phi} \\ &= \frac{4\pi R^2 C\sin(\theta)}{4\pi R^2 C} = \sin(\arcsin\left(\frac{R_*}{a}\right)) = \frac{R_*}{a} \end{aligned} \tag{2}$$

Which is the result quoted earlier. Note that we have included a factor of $R^2\sin(\phi)$ to account for the differential area on the surface of a sphere.

Now let us say that we know something about the orientation of the system. For example, say that the orientation has been measured to be evenly distributed within the range $I \pm \sigma$. Since it is evenly distributed, the PDF would be constant over this interval, and would appear as a long box on the parameter map. The transit probability would then

be

$$P_{tr} = \frac{\int_{90°-\theta}^{90°+\theta} \int_0^{360°} p(\phi,\lambda) R^2 \sin(\phi)\ d\lambda\ d\phi}{\int_0^{180°} \int_0^{360°} p(\phi,\lambda) R^2 \sin(\phi)\ d\lambda\ d\phi} = \frac{\int_{90°-\theta}^{90°+\theta} \int_0^{360°} C(\phi) R^2 \sin(\phi)\ d\lambda\ d\phi}{\int_0^{180°} \int_0^{360°} C(\phi) R^2 \sin(\phi)\ d\lambda\ d\phi} \tag{3}$$

$C(\phi)$ is the box-shaped PDF of I, and can be written as the product of two Heaviside step functions

$$C(\phi) = \frac{H[\phi + (-I+\sigma)]\ H[-\phi + (I+\sigma)]}{2\sigma}. \tag{4}$$

The exact transit probability will depend on the specific values of I and σ. For example, a planet orbiting its parent star in the habitable-zone at a relative distance of $R_*/a = 1/215$ and with a box-shaped orientation measurement of $90° \pm 2.5°$ will have a transit probability of 0.107. A Hot Jupiter with the same orientation measurement, but with $R_*/a = 1/10$, has a transit probability of 1 since it is so close to its parent star. These probabilities are 21 and 10 times greater, respectively, than the transit probabilities in the absence of orientation information.

Usually, the uncertainty on a measurement will not be "box-like" as in the previous example, but Gaussian (Figure 2). For an orientation measurement of $I \pm \sigma$, this implies a Gaussian PDF of

$$p(\phi,\lambda) = \frac{1}{\sqrt{2\pi\sigma^2}} \exp\left[\frac{-(\phi - I)^2}{2\sigma^2}\right] \tag{5}$$

In this case, the transit probability is then

$$P_{tr} = \frac{\int_{90°-\theta}^{90°+\theta} \int_0^{360°} \frac{1}{\sqrt{2\pi\sigma^2}} \exp\left[\frac{-(\phi-I)^2}{2\sigma^2}\right] R^2 \sin(\phi)\ d\lambda\ d\phi}{\int_0^{180°} \int_0^{360°} \frac{1}{\sqrt{2\pi\sigma^2}} \exp\left[\frac{-(\phi-I)^2}{2\sigma^2}\right] R^2 \sin(\phi)\ d\lambda\ d\phi}, \tag{6}$$

As an example, an Earth-like planet at a distance of $R_*/a = 1/215$ with $\theta = \arcsin(1/215)$, orbiting a Sun-like star with a measured orientation of $90° \pm 2.5°$ would have a transit probability of

$$P_{tr} = \frac{\int_{90°-\theta}^{90°+\theta} \int_0^{360°} \frac{1}{\sqrt{2\pi\sigma^2}} \exp\left[\frac{-(\phi-90)^2}{2(2.5)^2}\right] R^2 \sin(\phi)\ d\lambda\ d\phi}{\int_0^{180°} \int_0^{360°} \frac{1}{\sqrt{2\pi\sigma^2}} \exp\left[\frac{-(\phi-90)^2}{2(2.5)^2}\right] R^2 \sin(\phi)\ d\lambda\ d\phi} = 0.085. \tag{7}$$

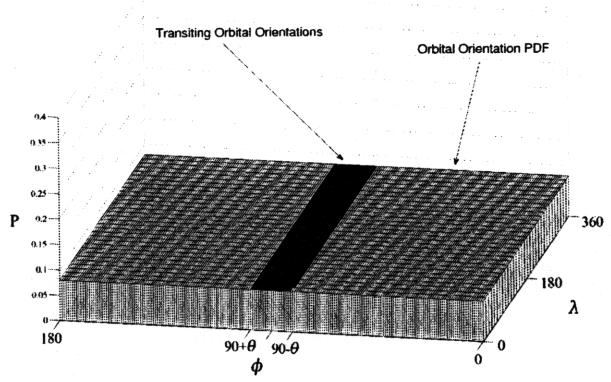

Fig. 1.— A "map" of the possible orbital orientations. With no prior orientation information, the probability density function is evenly distributed across this map. The shaded region shows the set of orientations that transit. Note that this map is distorted, and does not accurately show the effect of $\sin\phi$ at high latitudes.

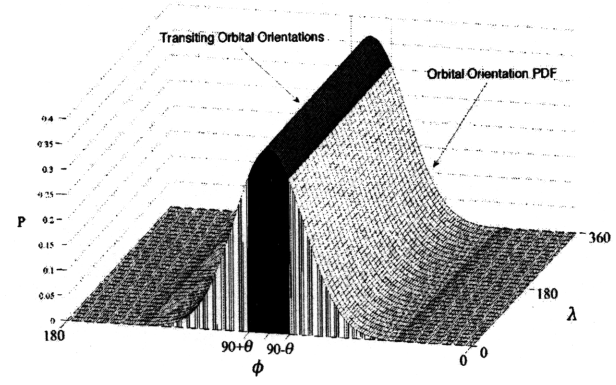

Fig. 2.— A "map" of the possible orbital orientations. In this case, a measurement has been made of the system's orientation, and so the probability density function is now shaped like a Gaussian. The shaded region shows the set of orientations that transit. Note that this map is distorted, and does not accurately show the effect of $\sin\phi$ at high latitudes.

This is about 17 times the base transit probability with no orientation information: 0.005. Figure 3 shows this increase relative to the base probability graphically for a range of orientation measurements of the form $I \pm \sigma$ assuming a similar orbital distance of $R_*/a = 1/215$. Figure 4 shows a similar plot for Hot Jupiters at a relative distance of $R_*/a = 1/10$.

Perhaps, however, we are not able to make a direct measurement of the distribution of I. As we will see, it is sometimes only possible to measure the value of $\sin(I)$. In this case, it is necessary to transform the measured distribution (presumably a Gaussian) into a distribution for I. To do this, we may make use of the fact that the differential area of both the original and the transformed distributions must remain the same so as to conserve probability. In the general case, where we have a distribution for the variable x, but would like to find the probability distribution of the function $y = g(x)$, the change of variables is given by

$$|f_Y(y)dy| = |f_X(x)dx|. \tag{8}$$

We may manipulate this to

$$f_Y(y) = \left|\frac{dx}{dy}\right| f_X(x) = \left|\frac{1}{g'(x)}\right| f_X(x) = \left|\frac{1}{g'(g^{-1}[y])}\right| f_X(g^{-1}[y]). \tag{9}$$

This allows us to convert between distributions for measurable quantities like i and $sin(i)$. Using a change of variables also gives another method to calculate the transit probability of a system. Consider the geometry of a transiting planet; the impact parameter, b, is the projected star-planet separation seen by the observer. It is typically normalized to the parent star's radius, so that $b = 1$ corresponds to a planet that just grazes the edge of the stellar disk. Mathematically,

$$b = \frac{a}{R_*}\cos(I). \tag{10}$$

For a transit to occur, b must be less than one. Therefore, if we have a probability distribution $f_B(b)$ for the impact parameter, the probability of the system showing a transit

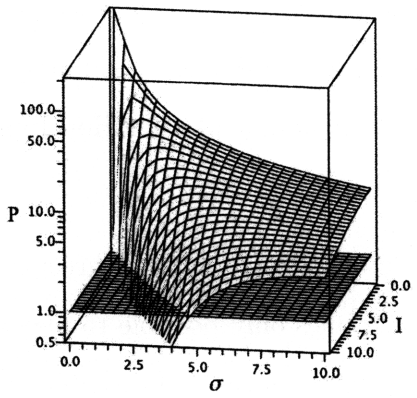

Fig. 3.— The relative transit probability (the probability with measurement divided by the probability with no measurement) of a habitable-zone planet with $R_*/a = 1/215$ and Gaussian orientation measurements of the form $I \pm \sigma$. Note that a flat plane at a factor of 1 has been included for reference.

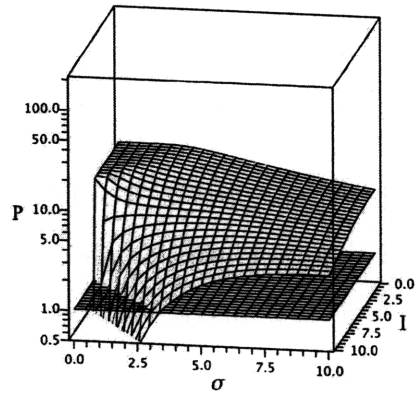

Fig. 4.— The relative transit probability (the probability with measurement divided by the probability with no measurement) of a Hot Jupiter with $R_*/a = 1/10$ and Gaussian orientation measurements of the form $I \pm \sigma$. Note that a flat plane at a factor of 1 has been included for reference.

will be the same as the probability that $b < 1$, or

$$P_{tr} = \int_0^1 f_B(b) db. \tag{11}$$

How do we arrive at the function $f_B(b)$? It is possible to make measurements of I and $\sin(I)$ - to arrive at probability distributions for these two quantities - but it is not possible to measure b without actually seeing a transit. The answer is to make a change of variables using equation (9). Say, for example, that we have measured a distribution for the inclination of the planetary system, $f_I(I)$. Using this distribution and equation (10), we may make a change of variables such that

$$f_B(b) = \frac{R_*/a}{\sqrt{1 - \frac{R_*^2}{a^2} b^2}} f_I \left(\arccos \left[\frac{R_*}{a} b \right] \right). \tag{12}$$

Similarly, if we have measured a distribution for the value of $\sin(I)$ as $f_S(\sin(I))$, then the distribution function for the impact parameter will be

$$f_B(b) = \frac{R_*/a}{\sqrt{1 - \frac{R_*^2}{a^2} b^2}} \left| \frac{R_*}{a} b \right| f_S \left(\sqrt{1 - \frac{R_*^2}{a^2} b^2} \right). \tag{13}$$

In practice, it is more useful to transform a distribution for a measurement of $\sin(I)$ into a distribution for I. As described in Section 2.4, accounting for the possible range of planetary system inclinations is easiest done using a distribution of the angle I.

In addition to changing variables, we must also consider how, from a Bayesian perspective, measurement of the stellar orientation influences the distribution of $f_I(I)$ and $f_B(b)$. Any measurements we make will be an additional piece of information that we will add on to our prior assumption that the orbits are randomly oriented in space. According to Bayes' Theorem, the updated distribution will depend on the measured distribution $f_{I,m}$ and the prior distribution $f_{I,p}$ as

$$f_{I,u} = \frac{f_{I,m}\ f_{I,p}}{\int_{0^\circ}^{90^\circ} f_{I,m}\ f_{I,p}\ di} \tag{14}$$

In the case of very precise observations, such as asteroseismology, the measurement will swamp the prior, and the resulting updated distribution will be very close to the measured distribution. For less precise measurements, such as determining the stellar orientation through spectroscopic measurement of $v\sin(I)$, the prior distribution has a noticeable effect on the updated distribution.

2.2. Measuring Stellar Inclinations: $v\sin(I)$

One way to measure the inclination of stellar rotation axes is by observing the projected stellar rotation rate, $v\sin(I)$. This is almost always measured spectroscopically, by looking for and interpreting the widening of a star's spectral lines. Unfortunately for many applications, the spectroscopy can only tell what the rotational velocity is projected on the plane of the sky; a star rotating pole on to an observer on Earth would show $v\sin(I) = 0$. For the purposes of finding the orientations of a star however, the projection is advantageous. Assuming that one could measure the true rotational period of the star by observing periodic photometric variation, and had an estimate of the star's radius, it would be possible to calculate the sine of the orientation angle I of the star's equator,

$$\sin(I) = \frac{PW}{2\pi R}. \tag{15}$$

Here, P is the measured true rotational period of the star, and R is the stellar radius. For clarity, the measurable quantity $v\sin(I)$ has been replaced by the variable W. Assuming that the measurements of P, R, and W have Gaussian errors (σ_p, σ_R, and σ_W respectively), and that the fractional errors are on the order of 10% or lower, we may calculate the expected error on the value of $\sin(I)$ by standard error prorogation;

$$\sigma_{\sin(I)} = \frac{PW}{2\pi R}\sqrt{\left(\frac{\sigma_P}{P}\right)^2 + \left(\frac{\sigma_R}{R}\right)^2 + \left(\frac{\sigma_W}{W}\right)^2}. \tag{16}$$

The PDF of $\sin(I)$ — f_S — is then a Gaussian with mean μ given by equation (15) and σ by equation (16). Per the previous derivation of transit probabilities, it is helpful to transform this into a distribution for I. To do this, we make use of equation (9) to change variables, and get

$$f_I(I) = |\cos(I)| \cdot f_S(\sin[I]). \tag{17}$$

To take a specific example, Winn et al. (2007) measured a 13.4 ± 0.4 day variation in the light curve of HD 189733 while observing the star to measure the system's spin-orbit alignment. In their paper, the authors hypothesize that this is the true rotational period of HD 189733. Together with their measurements of $v \sin(I) = 2.97 \pm 0.22 \mathrm{km\ s^{-1}}$ and $R = 0.753 \pm 0.025 R_\odot$, they calculate that $\sin(I) = 1.04 \pm 0.09$. If this measurement has Gaussian errors, then the implied distribution for the values of $\sin(I)$ may be transformed into a distribution for I as above. The resulting distribution (Figure 5) is then

$$f_{I,m}(I) = \left(\frac{|\cos(I)|}{\sigma\sqrt{2\pi}} \exp\left[\frac{-(\sin(I) - \mu)^2}{2\sigma^2} \right] \right), \tag{18}$$

Note that the distribution of I as shown in Figure 5 is not a Gaussian; the flatness of the sine function near ninety degrees mean that small uncertainties in the value of $\sin(I)$ translate into large uncertainties in the value of I Indeed, even though Winn et al. (2007)'s measurement of $\sin(I)$ has a fractional error of 9%, there is only a 50% chance that HD 189733 has an inclination of greater than 68°. Using equation (18) to update our prior distribution for i that assumes randomly oriented orbits, the updated distribution $f_{I,u}$ of the stellar inclination is now

$$f_{I,u}(I) = \frac{\left(\frac{|\cos(I)|}{\sigma\sqrt{2\pi}} \exp\left[\frac{-(\sin(I)-\mu)^2}{2\sigma^2} \right] \right) \sin(i)}{\int_0^{90} \left(\frac{|\cos(I)|}{\sigma\sqrt{2\pi}} \exp\left[\frac{-(\sin(I)-\mu)^2}{2\sigma^2} \right] \right) \sin(i)\ di}. \tag{19}$$

If we integrate this using the equations described in the previous section on transit probabilities from $(90° - \arcsin(R_*/a)) \leq I \leq 90°$, and using using HD 189733 b's relative

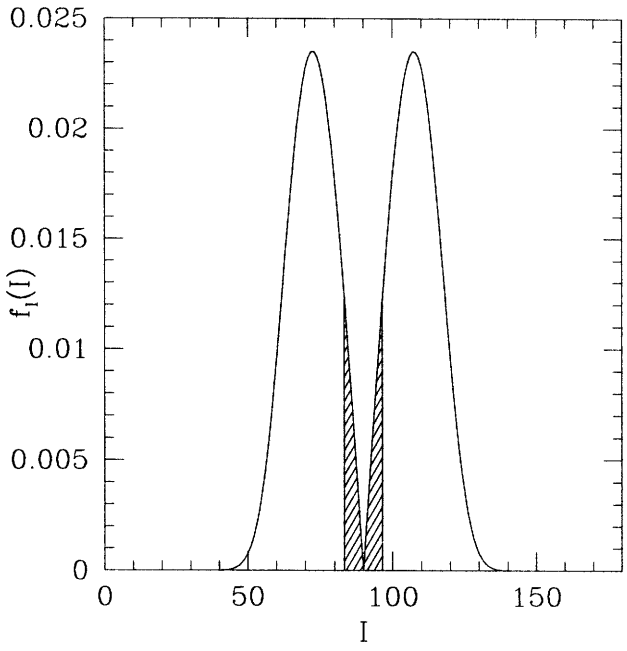

Fig. 5.— The measured distribution $f_{I,m}(I)$, the inclination of the stellar equator of HD 189733, using the measurement of $\sin(I)$ made by Winn et al. (2007). The shaded region is the range of angles that allow for transits.

orbital distance of $R_*/a = 1/8.89$, then Winn et al. (2007)'s measurement of $\sin(I)$ gives a transit probability of 30%. Note that this probability does not take into account the inclination of the planetary system; we have assumed that the orbit of HD 189733 b is co-planar with the stellar equator.

Typically, it is possible to measure P, R and W with a precision of several percent. The most common way to measure the true rotational period of the star, as in the case of HD 189733, would be by photometrically observing periodic variation in the light curve. Presumably, this would be the result of a long-lived star-spot on the stellar photosphere. This should allow the rotational period of the star to be determined to within 5% (Arentoft et al. 2008; Winn et al. 2007). Complications arise from the fact that what is observed may be an alias of the true period. Indeed, Arentoft et al. (2008) observed photometric variation of Procyon with a period of 10.3 ± 0.5 days, but found it much more likely that the rotational period of Procyon is twice that, at 20.6 ± 1.0 days. Furthermore, if the variation is caused by a star-spot, differential rotation of the stellar photosphere may distort the true value of the period. On the Sun differential rotation means that a sun-spot half-way between the solar equator and pole has a period 5% longer than a sun-spot on the solar equator. More troubling from the perspective of identifying a transiting planet, the photometric variability that would enable the determination of a star's rotational period could drown out the signal of the transit. Therefore, while the formal error on measurements of P may be $3 - 5\%$, there may be systematic errors that make the true precision of the measurement worse.

In general, the stellar radius may only be measured indirectly. Typically radii are estimated by taking spectroscopically measured values of the effective temperature, surface gravity, and metallicity and combining these with observations of a star's bolometric luminosity to place the star on a set of theoretical stellar evolutionary tracks. For the bright stars that ExoPlanetSat will observe estimation of stellar radii will be made easier by the

availability of Hipparcos parallaxes for all of the potential targets. Having the distance to the target stars allows for much more precise determinations of the star's bolometric luminosity. All together, it is generally possible to estimate stellar radii to within 5%.

In contrast to P and R, which can be discussed with fractional errors, for velocities of less than 30 km/s the error on measurements of W are usually constant in absolute (and not percentage) terms at about ± 0.25 km/s. For solar-like stars, with surface rotational speeds on the order of 2 km/s, this means that it would be very difficult to measure W to better than 12%. This occurs because the manner in which W is measured. The surface of a rotating star is Doppler shifted due to its rotational velocity; blue shifted on the half approaching the observer, and red-shifted on the half receding from the observer. This has the effect of broadening the star's spectral lines, since the integrated light from the disk of the star is "blurred" by the Doppler shifting. This is also why the surface rotation is measured as $v \sin(I)$, since a star with $I = 0$ would be pole-on to the observer, and display no Doppler shift from its rotation. Unfortunately, many other processes, such as pressure broadening, turbulence, and the thermal motion of the atoms in the photosphere broaden spectral lines. The result is that even an ideal non-rotating star would not display perfectly sharp absorption lines, and this unavoidable pressure and thermal line-broadening is what places the noise floor on measurements of W, as it is indistinguishable from rotational broadening. For solar-like stars, with surface rotational speeds on the order of 2 km/s, this means that it would be very difficult to measure W to better than 12%.

Together with what we may reasonably expect as the fractional uncertainties on the measurements of P and R, a fractional uncertainty in W of 12% means that measurements of $\sin(I)$ of a solar-like star will usually have uncertainties of 10-15%. In the example of HD 189733, Winn et al. (2007) measured $\sin(I)$ to within 8.5%, which is better than what can be expected on average, due to their precise spectroscopic measurement of $v \sin(I)$.

Assuming the best case scenario, that we measure a mean of $\sin(I) = 1$ with an uncertainty of 10%, this would imply an updated distribution for I of

$$f_{I,U}(I) = \frac{\left(\frac{|\cos(I)|}{(0.1)\sqrt{2\pi}} \exp\left[\frac{-(\sin(I)-1)^2}{2(0.1)^2}\right]\right)}{\int_0^{90}\left(\frac{|\cos(I)|}{0.1\sqrt{2\pi}} \exp\left[\frac{-(\sin(I)-1)^2}{2(0.1)^2}\right]\right)\sin(i)\ di}. \quad (20)$$

For Hot Jupiters, with $R_*/a = 1/10$, this gives a transit probability of 21.5%. For habitable-zone planets, with $R_*/a = 1/215$, the transit probability is 1%. These probabilities are both about twice what they would be in the case of no information about the orientation of the star (10% and 0.5%, respectively). Given the fractional noise floor on measurements of $v \sin(I)$ of 12% using conventional methods, obtaining better precision may only be achievable with specialized observations, such as interferometric spectroscopy that resolves the different sides of the stellar disk.

2.3. Measuring Stellar Inclinations: Asteroseismology

Another way to measure the inclination of a star is through asteroseismological observations, which we describe in summary below. These observations use high-cadence precise radial velocity or photometric observations to measure pulsations of the stellar photosphere. These pulsations are much lower amplitude than those that drive variable stars; typically they have radial velocity amplitudes of cm s^{-1} or m s^{-1}. For many years heliosiesmologists have studied pulsations with similar amplitudes in the Sun. It was only ten years ago that Martić et al. (1999) were first able to identify solar-like pulsations in the power spectrum of another star (Procyon in this case); this was largely enabled by the creation of highly precise spectrographs and photometers for planet-finding surveys (Bedding & Kjeldsen 2008).

There are several different types of pulsations that asteroseismologists measure. The

ones that allow for the determination of the stellar inclination are the p-mode non-radial pulsations. The p-modes are distinct from the g-mode pulsations because they are caused by pressure (hence p-) waves generated by internal fluctuations within the convective zones of the star. They are acoustic waves traveling through the star's interior. The g-modes are gravity waves, and for solar-like stars are largely confined to the radiative areas in the stellar core. The p-modes themselves are further divided into radial and non-radial pulsations. Radial pulsations are what typically occur in variable stars such as Cepheids or RR Lyrae stars: the expansion and contraction of the entire stellar photosphere. Non-radial pulsations are, as the name implies, not a radial "breathing" in-and-out of the photosphere but a series of spherical harmonics with different modes, each of which is denoted by the variables (n, l, m).

The non-radial modes allow for the determination of the stellar inclination precisely because they are described by spherical harmonics. The reasons lies in the azimuthal number, m. In the ideal case of a non-rotating star, for a given (n, l) all of the different m orders are degenerate and lie exactly on top of one another in the power spectrum. Thus, if we could observe a non-rotating (or pole-on) star, we would only see peaks in the power spectrum corresponding to different values of (n, l). On the other hand, if the star is rotating, then the m orders split in frequency space so that we would now see peaks corresponding to the different values of m clustered around the locations of the (n, l) peaks that we see in the non-rotating case. Each degree l has $(2l + 1)$ possible values of m (the integer values from $-l$ to l), so that the dipole with $l = 1$ has three allowable values for m, the quadrupole with $l = 2$ has five, and so on.

By measuring the frequency offsets of the different m orders from their central $m = 0$ peak, it is possible to also measure the angular velocity of the star. If the angular velocity of the star is small and we assume rigid body rotation, then to first order the shifted

frequencies of the different m modes are (Ledoux 1951)

$$\omega_{nlm} = \omega_{nl} + m\Omega(1 - C_{nl}), \tag{21}$$

where Ω is the rotational frequency of the star. This is commonly referred to as "rotational splitting" of the acoustic modes. The dimensionless factor C_{nl} corrects for the Coriolis effect, and for solar-like oscillations is typically very small ($C_{nl} < 10^{-2}$) (Gizon & Solanki 2003). Note that the rotational splitting will not be a linear function of m if there is differential rotation on the surface of the star (i.e. Ω varies with latitude). To first order therefore, by measuring the amount of rotational splitting in a star's asteroseismological power spectrum it is possible to calculate the rotational frequency of the star, Ω, and by extension the rotational period of the star $p = \Omega^{-1}$.

Alternatively, Gizon & Solanki (2003) (see also Ballot et al. (2008)) derive the relative power of the different (l, m) eigenmodes as a function of the stellar inclination angle. For the dipole ($l = 1$) modes they calculate that relative powers $\varepsilon_{l,m}$ of the modes are

$$\varepsilon_{1,0} = \cos^2(I) \tag{22}$$

$$\varepsilon_{1,\pm1} = \frac{1}{2}\sin^2(I), \tag{23}$$

and for the quadrupole modes ($l = 2$) they derive

$$\varepsilon_{2,0} = \frac{1}{4}(3\cos^2(I) - 1)^2 \tag{24}$$

$$\varepsilon_{2,\pm1} = \frac{3}{8}\sin^2(2I) \tag{25}$$

$$\varepsilon_{2,\pm2} = \frac{3}{8}\sin^4(I). \tag{26}$$

Therefore by measuring the ratio of the power in different orders m it would also be possible to calculate the stellar inclination angle.

Asteroseismological observations using radial velocity measurements are able to pick out the $l = 1$, $l = 2$, and $l = 3$ modes. This is in contrast to photometric asteroseismic

observations, which can usually only pick out the $l = 1$ and $l = 2$ modes. The difference arises because the radial velocity measurements manage to partially resolve the approaching and receding portions of the stellar disk through the rotational broadening of the spectral lines. This is conceptually similar to the way in which the Rossiter-McLauglin effect allows one observe the progressive eclipse of different parts of the stellar disk. In any event, by partially resolving the stellar disk, radial velocity observations are more sensitive to higher order modes which would otherwise tend to cancel themselves out in an integrated measurement of the disk. Radial velocity measurements are also less sensitive than photometry to granularity on the photosphere of the target star (T. Campante, private communication). Granulations introduces an unavoidable jitter into photometric observations, and raises the background noise level. Since spectra are not as affected by the granulation, asteroseismological observations in radial velocity have a lower level of background noise.

The Stellar Observations Network Group (SONG)[1] project aims to use radial velocity observations to make asteroseismological observations. The key to the SONG idea is a network of eight 1m telescopes placed around the world. This will allow SONG to observe a target star continuously. Uninterrupted monitoring of a star is vital to taking precise, high resolution asteroseismological observations. The typical frequency spacings of solar-like oscillations are on the order of 0.5μhz, and to achieve the resolution necessary to distinguish the different oscillation modes, one needs a high cadence and long time-baseline set of observations. See, for example, Bazot et al. (2007), who used five nights on the HARPS spectrograph to observe α Cen, but were stymied by the limited time-baseline and daily interruption of their observations, which reduced the resolution of their power spectrum. The SONG group also plans to increase the accuracy of their fits to the data by conducting

[1]See http://astro.phys.au.dk/SONG/ for a more detailed description.

"global fits," as opposed to fitting each multiplet mode by itself. SONG will fit 10 to 15 multiplets simultaneously, which will allow the group to derive asteroseismic parameters to a high accuracy and precision.

An exact determination of the precision expected from the SONG measurements is the subject of future work. In the mean time, we have used the internal estimates by the SONG team of their achievable precision (T. Campante, private communication), coupled with the analysis of photometric asteroseismology data by Gizon & Solanki (2003) and Ballot et al. (2008). From these, we estimate that the asteroseismological observations that will be conducted by SONG should be precise enough to determine the angle of stellar rotation to within 2.5°. This means, for Gaussian errors, that a habitable-zone planet with $R_*/a = 1/215$ that is orbiting a star with a SONG-provided orientation measurement of $I = 90° \pm 2.5°$ will have a transit probability of 8.5%, which is 17 times greater than the transit probability for a habitable-zone planet with no prior information about the orientation of the stellar spin-axis. The true transit probability, however, will be less than 8.5%, since we have not yet accounted for the possible inclination of the planetary system itself.

2.4. Planetary Inclinations

The entire preceding discussion of transit probabilities and of measuring the orientation of a star's rotation has made the same tacit assumption; namely that any orbiting planets are coplanar with the stellar equator. From the Solar System we know that this is not necessarily the case. The ecliptic is inclined by 7.155° (Beck & Giles 2005) to the Sun's equator. For extrasolar planets it has been possible to make a partially similar measurement of the spin-orbit alignment of exoplanetary systems in the plane of the sky (see e.g., Winn et al. (2006)), though no direct measurements have been made of the true three-dimensional

spin-orbit alignment. Nevertheless, it is reasonable to assume that exoplanetary systems will not be co-planer with their parent star's equator.

For transiting planets it is possible to measure the inclination of exoplanetary orbits to their parent star's equator in the plane of the sky through the Rossiter-McLaughlin effect. The Rossiter-McLaughlin effect has a distinct signature in the spectroscopic radial velocity curve of a system that occurs during a planetary transit. It occurs because as seen from Earth, the photosphere of a rotating star is partially blue-shifted (on the half that is seen rotating towards the Earth) and partially red-shifted (on the half rotating away from the Earth). For well-aligned systems, as the planet passes in front of the star, it partly obscures first one side and then the other and causes the stellar spectrum to undergo a Doppler shift first towards the red (when the planet is obscuring the blue-shifted side) and then towards the blue (when it is over the red-shifted side). In a spectroscopic radial velocity curve, this looks like a characteristic up-and-down in the radial velocities. In an unaligned system, the dip will become less pronounced and for planets transiting away from the stellar center, less symmetric.

By measuring the magnitude and shape of these dips, it is possible to measure the alignment on the plane of the sky between the projected rotation axis of the star and the projected orientation of the planetary orbit (Ohta et al. 2005), the projected "spin-orbit angle." While this does not yield any information about the orientation of the star along our line of sight, Fabrycky & Winn (2009) combined spin-orbit measurements from eleven exoplanetary systems in an attempt to determine the distribution of the three-dimensional planetary inclinations.

That being said, the data that Fabrycky & Winn (2009) use are only based on observations of Hot Jupiters, and so may not be applicable to the habitable-zone planets that ExoPlanetSat is designed to find. We have instead made the assumption that the

inclination of planetary systems are evenly distributed within 5° of the stellar equator. This is admittedly arbitrary, but until the equivalent paper to Fabrycky & Winn (2009) can be written about habitable-zone planets, we feel that it is a reasonable assumption to make.

t is illustrative to see how this distribution affects transit probabilities. Factoring in the inclination of the exoplanetary system, the inclination as observed from Earth will be $i = I - \psi$, where I is the inclination of the stellar equator, and ψ is the inclination of the planetary system to the equator. The distribution of the angle i is then

$$f_i(i) = \int_{-\infty}^{\infty} f_J(I, I - i) dI, \tag{27}$$

where $f_J(I, I - i)$ is the joint distribution of I and ψ, and $I - i$ has been substituted in place of ψ. Since I and ψ are independent variables, their joint distribution is simply the product of their individual distributions: $f_J = f_I \cdot f_\Psi$. Thus, the distribution of i will be

$$f_i(i) = \int_{-\infty}^{\infty} f_I(I) f_\Psi(I - i) dI, \tag{28}$$

Including the spread of possible system inclinations into the calculations of transit probabilities acts to spread out the resulting distributions. For a stellar orientation determined using spectroscopic measurement of $\sin(I)1.0 \pm 0.1$ the transit probability for a habitable-zone planet with $R_*/a = 1/215$ is over six times lower, at 0.16%. If we have an asteroseismological measurement of the stellar orientation of $I = 90° \pm 2.5°$, and again assume planetary inclinations that are uniformly distributed within 5°, then the transit probability for a habitable-zone Earth orbiting a Sun-like star is higher: 5%. This is an order of magnitude greater than the transit probability for a habitable-zone planet with no prior information about the orientation of the system. For the design of the ExoPlanetSat survey, this is what we will assume is the transit probability of a habitable-zone Earth.

3. Optical and Instrumental Design

Ideally, the ExoPlanetSat spacecraft will be designed with the smallest telescope capable of detecting an Earth-sized transit around a bright star. In detail there are several points to consider when designing the spacecraft's optical system. Firstly, ExoPlanet will image stars spanning a range of magnitudes; the design will have to be sufficient for detection with the dimmest stars, but also prevent saturation of the brighter stars. Secondly, the effect of noise in the data, particularly the effect of a noise floor from spacecraft jitter or other systematics, will push the telescope towards a larger size than the ideal shot-noise limited case, so as to lower the statistical noise and keep the total uncertainty in the data at the same level. Finally, ExoPlanetSat may end up using a standardized nanosatellite housing, which will limit the size of the telescope and optical system *a priori*.

3.1. Background

The two most basic quantities that we would like to design for are the pupil diameter (D) and the focal length (f) of the optical system. Since ExoPlanet Sat is small, it is practical to design the telescope to use refractive optics. Indeed, the secondary mirror of a reflective system would reduce the light gathering area of the telescope, and the spider support struts would cause unwanted diffraction spikes on the final images. Therefore, we would like to design for the diameter and the focal length of the lens of the spacecraft's telescope. Also of interest is the overall "f-ratio" of the telescope, which is defined as the ratio between the focal length and the diameter of the optic, in this case the lens. It is conventionally written as $f/ = F/D$.

Most basic optic designs make the assumption that all of the incoming light rays are close enough to the optical axis (both angularly and linearly) that the sines and tangents of

angles are equal to the angles themselves. This is known as the "paraxial approximation." To first order this is a valid approximation; for example, within a 5 degree field of view, the paraxial approximation would cause errors of only 0.2% at the edge of the field.

The "plate scale" of the optical system is another important quantity. The term comes from the use of photographic plates for astronomical observations, but its meaning remains that same for CCD imaging: the height in the focal plane of an object with angular extent θ. From the basic arrangement of the optical system, we may say that the tangent of this angle θ will be equal to

$$\tan(\theta) = \frac{y}{f}, \tag{29}$$

where y is the height in the focal plane, and f is the focal length. By the paraxial approximation, $\tan(\theta) \approx \theta$, and we may rewrite equation (29) as

$$\frac{\theta}{y} = \frac{1}{f} = \text{plate scale.} \tag{30}$$

The plate scale is usually quoted in units of arcseconds per μm, or in arcseconds per pixel - the conversion depends on the physical size of a detector's pixels.

The field of view of the detector is directly calculable from the plate scale, as well as from consideration of geometrical optics. From the plate scale, one only needs to multiply the calculated scale by the size of the detector (in either physical units or in pixels), to arrive at the size of one side of the field of view. In other words, if d is the size of the detector,

$$\theta_{FOV} = d\left(\frac{\theta}{y}\right) = \frac{d}{f}. \tag{31}$$

Alternatively, we may also derive this result from a result of geometrical optics, that the etendue of a telescope (the area and solid angle of a beam) is conserved as it passes through an optical system. At the entrance to the telescope, the area of the beam is $A = \pi D^2/4$, and the solid angle covered by the beam is $\Omega = \pi\theta_{FOV}^2/4$. At the surface of the detector,

the beam has shrunk to $A = \pi d^2/4$, while the solid angle has changed to $\Omega = \pi[1/(f/)]^2/4$. Equating these two values of $A\Omega$ gives the relation

$$D(\theta_{FOV}) = \frac{d}{f/}, \tag{32}$$

which reduces to equation (31).

3.2. Expected Photon Counts

The primary driver of the ExoPlanetSat optical system is the requirement that the spacecraft be able to detect the transit of an Earth-sized planet in front of a bright solar-type star. This results in several instrumental requirements, but the most immediate is the need to collect enough photons for the shot noise to drop to allowable levels. Therefore, we determined the expected photon counts the spacecraft will observe. For design purposes, we scaled each star to be at a V-magnitude of $m_V = 6$. Note that V-band is not what we have chosen for the ExoPlanetSat bandpass, which is 400-1000nm, and is only used as a convenient reference.

All other things being equal, the photon count rate for an instrument may be estimated by integrating a blackbody spectrum of the appropriate temperature under the correct bandpass, and applying the relevant response functions for the filter and CCD. In reality, however, stellar spectra are not blackbodies. We have corrected for this effect by directly integrating spectral templates over ExoPlanetSat's bandpass of 400-1000nm.

The spectral templates that we used were based on the Kurucz model stellar atmospheres (Kurucz 1979). The versions we used were from the STSCI Calibration Data System[2], and were already unpacked into ascii files containing a wavelength column and a

[2]http://www.stsci.edu/hst/observatory/cdbs/k93models.html

surface flux (erg s^{-1} cm^{-2} $Å^{-1}$) column. This is different from the versions available on the Kurucz model website[3], which hosts the packed files with units of the Eddington flux (erg s^{-1} cm^{-2} sr^{-1} hz^{-1}). To convert between the units, the relation is

$$F_{surf}(\lambda) = \frac{3.336 \times 10^{-19}\ \lambda^2}{4\pi} F_{Edd}. \tag{33}$$

As an example, Figure 7 shows the Kurucz model spectrum of a 5750K dwarf with solar metallicity and no α-enhancement. A blackbody spectrum for 5750K is overlaid.

Integrating the surface flux curves yields the stellar luminosity at the photosphere. To convert this to an observed flux some distance from that photosphere, we must then multiply the integrated surface flux by a factor of R_*/D, where R_* is the stellar radius, and D is the distance to the star. In the case that the radius of the star is not known, we used the temperature-radius relationship implicit in the Yonsei-Yale (Y^2) stellar isochrones (Yi et al. 2001) for the solar-metallicity zero-age main sequence, which we numerically determined to be

$$\log\left(\frac{R}{R_\odot}\right) = 5.4366X^3 - 56.166X^2 + 194.04X - 224.55 \tag{34}$$

where $X = \log(T_{eff})$.

As a check, we used the definitions in Allen's Astrophysical Quantities (Cox 2000), hereafter AAQ, for the Johnson-Cousins B- and V-bands (including AAQ's zero magnitude calibration point) to calculate B- and V-magnitudes for each of the templates (Figures 8 and 9). Generally, the calculated values were within 0.05 mag of the values in AAQ. Table 1 gives the calculated photon counts in the bandpass of ExoPlanetSat of 400nm to 1000nm for a variety of spectral types at a V-band brightness of $m_V = 6$.

---

[3]http://kurucz.harvard.edu

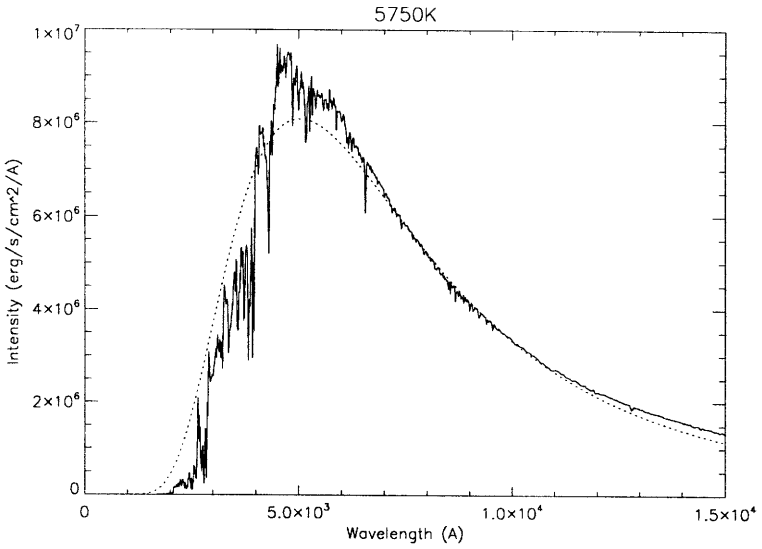

Fig. 6.— The Kurucz template spectrum (Kurucz 1979) for a 5750K dwarf star with solar metallicity and no α-enhancement, overlaid by a 5750K blackbody.

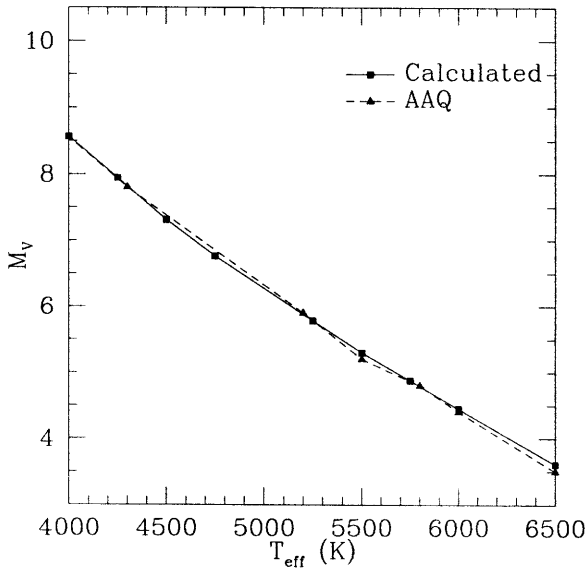

Fig. 7.— Absolute V-magnitudes calculated using the Kurucz template spectra (Kurucz 1979) versus absolute V-magnitudes from Allen's Astrophysical Quantities, Table 15.7 (Cox 2000).

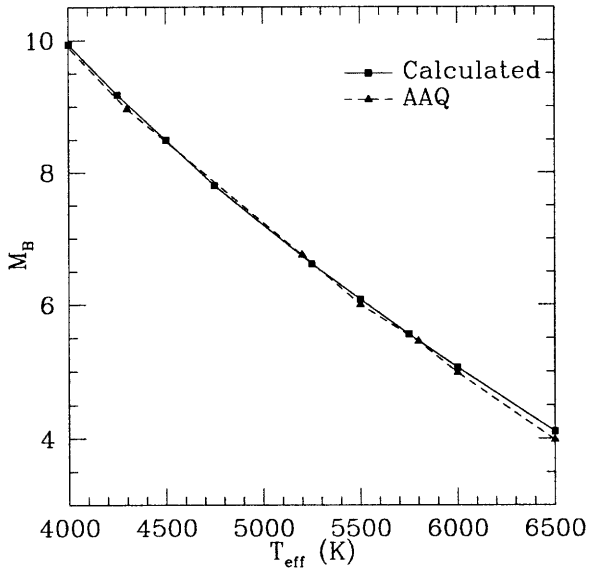

Fig. 8.— Absolute B-magnitudes calculated using the Kurucz template spectra (Kurucz 1979) versus absolute B-magnitudes from Allen's Astrophysical Quantities Table 15.7 (Cox 2000).

3.3. Aperture Requirements: Shot-noise Only

We first consider the design of the ExoPlanetSat spacecraft in the ideal case where photon counting statistics are the only noise in the data. To detect the transit of an Earth-sized planet in front of a Sun-like star, ExoPlanetSat will need to achieve high photometric precision, and to minimize the number of statistical false positives, we require that the spacecraft be able to detect the transit of an Earth-sized planet in front of a Sun-like star with a signal-to-noise (S/N) of ten. Since the signal of the transit is the fractional change in brightness of the target star during transit, the required precision in the photometric data is therefore

$$\sigma_{req} = \left(\frac{1}{10}\right)\left(\frac{R_\oplus}{R_\odot}\right)^2 = 8.4 \text{ ppm}. \tag{35}$$

Around less massive stars with smaller stellar radii the transit depth, and the minimally required precision, will be larger, but for the purposes of design we will take the solar case as our baseline since we expect early G-dwarfs to dominate ExoPlanetSat's target catalog. The required precision of 8.4 ppm allows us to set the minimum required aperture ExoPlanetSat's optical system.

When the only noise in the data is from the Poisson statistics of the collected photons, the precision of each exposure is just

$$\sigma = \frac{\sqrt{N_S}}{N_S}, \tag{36}$$

where N_S is the number of photons collected from the target star, and the factor of 1.0857 converts to the astronomical magnitude scale. This implies that ExoPlanetSat needs to collect $N_S = 1.67 \times 10^{10}$ photons to reach a precision of 8.4ppm.

Collecting this $N_S = 1.67 \times 10^{10}$ photons in a single exposure would far exceed the

500,000 e^{-1} full-well depth of the ExoPlanetSat CCDs,[4] and thus saturate the detectors. To prevent this from occurring, the science images will be deliberately defocused to spread the starlight out over approximately 100 pixels. Additionally, ExoPlanetSat will take several short exposures with less individual precision and then bin them together. The precision in the set of binned exposures will be

$$\sigma_{bin} = \frac{1}{\sqrt{n_{points}}}\,\sigma_{ind} = \sqrt{\frac{t_{exp}+t_{read}}{t_{tr}}}\,\sigma_{ind}, \tag{37}$$

where σ_{ind} is the precision of an individual exposure, t_{exp} is the exposure time, t_{read} is the read time of the CCDs, and t_{tr} is the time spent collecting in transit data. For the frame transfer CCDs that ExoPlanetSat will use the read-out time t_{read} is the time it takes to shift the image onto the covered half of the CCD, and is under a millisecond - effectively zero. The total in transit observing time, t_{tr} is dependent on the total amount of time that ExoPlanetSat looks at the target star, and the duration of the transit itself. In a nominal mission ExoPlanetSat will stare at a target for one third of its 90 minute orbit. For an Earth-analog with a transit duration of 13 hours, this will give a total observing time of 4.3 hours per transit. More generally, the in transit observing time is given by the relation

$$t_{tr} = f_{orb} t_{obs} \frac{R_*}{\pi\, a}, \tag{38}$$

where we have included the factor f_{orb} to account for the spacecraft only being able to stare at a target for a fraction of an orbit.

Since the read-out time of the CCDs is near zero, to first order the exposure time, t_{exp}, cancels out in the calculation of the binned data precision. We have therefore set the exposure time to a fiducial value of 10 seconds. This will ensure that the ExoPlanetSat CCDs do not saturate while imaging the brighter targets. Using other values yields very

[4]The CCD choice and the focal plane design are described in more detail in Section 3.5.

small changes in the precision of the ExoPlanetSat data; on the order of 0.05% for a change to 30 seconds.

For the purposes of the spacecraft design, we will use the counts for a G2V star as our fiducial case. This will enable the spacecraft to also detect the deeper transits of Earth-like planets around smaller stars. Also, because the ExoPlanetSat target catalog will be a magnitude limited set of the nearby G- and K-dwarfs, we expect that dwarf stars earlier than G5V will be half of the list of potential targets.

To fill out the "trade-space" of the design, we have considered a G2-dwarf in several different magnitude ranges. As a baseline, let us consider what aperture is required to detect the transit of an Earth-sized planet across a G2-dwarf with apparent magnitude $m_V = 6$. This scenario presents a transit depth of 84ppm. As we can see from Table 1, at $m_V = 6$ a G2-dwarf has a count rate of 10,162 γ cm^{-2} s^{-1}. In figuring the aperture needed to capture an S/N=10 detection of this transit, the main determinant will be the photon count rate from the target star: N_S.

We may thus use equation (37) to determine the minimum aperture for a S/N=10 detection. Doing so, we find that we require 90.8cm^2 of effective collecting area (Figure 10). As a rough estimate, we will assume that the combined efficiency of the lens, filter, and CCD is 0.81. This is similar to the TESS satellite. With a combined efficiency of 0.81, ExoPlanetSat will require a lens that is 11.9cm in diameter for this baseline case of an $m_V = 6$ star. The first column of Table 2 shows the required diameters for other magnitude limits. Note that the exposure time, 10 seconds, is the same for all the magnitude bins. The second column in Table 2 is the result of similar calculations, but with a relaxation of the signal-to-noise requirement to S/N=7.

3.4. Aperture Requirements: With Other Noise

In the real world, there will be other noise sources contributing to the ExoPlanetSat data besides just photon counting statistics. The precision of the photometric data taken by the spacecraft will affected by several additional sources of uncertainty: instrumental noise, background light, stellar variability, and pointing jitter. Having previously calculated what the aperture requirements are for ExoPlanetSat in the case of no noise, we now factor in these noise sources to see what effect they will have on the size of ExoPlanetSat's telescope.

Instrumental: All though relatively small compared to other sources of noise, there will be instrumental noise from the dark current and read-noise of the CCDs. For the temperatures that we expect the ExoPlanetSat CCDs to operate at, 40-50°C. The dark current and read noise will be on the order of 5 e^- s^{-1} pix^{-1} of dark current and 2 e^- pix^{-1} of read noise (G. Ricker, private communication).

Background light: The background brightness of the sky will also contribute to the number of photons collected, and will mainly come from the blending of faint background stars for targets near the galactic plane, and from zodiacal light for targets near the ecliptic. Blending with fainter background stars can partially be accounted for by a detailed examination of the sky around each of the target stars. Unlike most photometric surveys, the targeted nature of ExoPlanetSat makes this a feasible task. The brightness of the target stars will also help to reduce the effects of blending. Since the zodiacal light varies across the sky, it is difficult to exactly say how much effect it will have on the precision of the photometric data without first knowing the location of the target star. We therefore have used the average value of the zodiacal light from Aldering (2001) as the baseline for zodiacal background. Using Aldering's blackbody approximation for the zodiacal light, we calculate that in the ExoPlanetSat bandpass (400-1000nm) the zodiacal flux is 1.87×10^{-21} erg cm^{-2} s^{-1} $arcsec^{-2}$, or 5.2×10^{-3} γ cm^{-2} s^{-1} $arcsec^{-2}$. The zodiacal flux falling onto

the pixels in the detectors will depend upon ExoPlanetSat's collecting area and the angular size of the CCD pixels, but for representative values of both these quantities (as described below) the zodiacal light provides a very small contribution - on the order of 0.02 counts per pixel on the science CCDs. This is far less than the number of counts expected from the stellar sources - about 100 counts per pixel. The small amount of background light is due to the defocusing of the science images, which spreads out the background, and to brightness of the science targets.

Stellar variability: Stellar variability adds an additional source of noise into the light curve. The variability can come from a number of sources, such as star spots or the stellar pulsations described in the previous section on asteroseismology. A detailed accounting for the amount of stellar variability that ExoPlanetSat can expect over the timescales of interest is unfortunately not yet available. We therefore use the value determined by Koch et al. (2000) for the Kepler mission - 10 ppm - as an estimate of the amount of stellar variability that we may expect to see in the ExoPlanetSat data over the timescale of 3 to 300 hours. The authors determined this value by combining solar variability observations in the literature with a sample of observations of other stars.

Spacecraft jitter: The ExoPlanetSat images will also be subject to noise that arises because of imperfections in the CCDs, both within individual pixels, and in between different pixels. To combat this noise source, we have taken two lines of attack. Firstly, the science images collected by ExoPlanetSat will be deliberately defocused. This will spread the image out over more pixels, and will therefore make the variations of individual pixels much less noticeable. Defocusing also has the added benefit that ExoPlanetSat can take longer science exposures without saturating the CCDs; a particular concern given the brightness of the target stars. Second, ExoPlanetSat will take relatively short exposures of 10 seconds, which will limit the amount of uncertainty jitter can contribute to any one

observation.

The jitter that the spacecraft experiences will contribute, along with other systematic effects, to the noise floor of the ExoPlanetSat data. Unlike the other sources of uncertainty discussed above, the effect of the noise floor on the photometric data cannot be removed by binning. Properly quantifying the amount of jitter and other systematic errors that ExoPlanetSat can expect to see will require detailed laboratory work using a replica of the ExoPlanetSat optical system. In lieu of such a set-up, we consulted published error budgets for the Kepler (Koch et al. 2000), CoRoT (Aigrain et al. 2009) and MOST (Reegen et al. 2006) missions.

We have taken the experimental results for the effect of jitter on the Kepler mission (Koch et al. 2000), and scaled the results to ExoPlanetSat. This allows us to define the pointing requirements for the spacecraft by working backwards from the maximum allowable jitter noise. The jitter amplitude, in units of pixels, scales as

$$\frac{\text{Jitter Ampl.}_{\text{EPS}}}{\text{Jitter Ampl.}_{\text{Kepler}}} = \frac{\text{Jitter Noise}_{\text{EPS}}}{\text{Jitter Noise}_{\text{Kepler}}} \sqrt{\frac{\text{Obs. Time}_{\text{EPS}}}{\text{Obs. Time}_{\text{Kepler}}}}. \tag{39}$$

The subscript "EPS" refers to ExoPlanetSat. The values determined by Koch et al. (2000) for Kepler are: $\text{Jitter Ampl.}_{\text{Kepler}} = 0.075\text{pix}$, $\text{Jitter Noise}_{\text{Kepler}} = 3\text{ppm}$, and $\text{Obs. Time}_{\text{Kepler}} = 300\text{min.}$ and using 30 minutes as the observing time for ExoPlanetSat

Since we are trying to calculate what pointing precision is required of the spacecraft, we approached the problem of spacecraft jitter and systematics from two different perspectives. Firstly, we have chosen two fiducial noise floors (10ppm and 50ppm) and examined their affect on the required aperture and achievable S/N of the spacecraft. Secondly, we have estimated the maximum allowable uncertainty that jitter and other systematics can contribute, given certain assumptions about the available aperture and desired S/N. In all the cases we alos use equation (refeq:3415) to determine the jitter amplitude in terms of fractions of a pixel.

If we add all of the additional noise from instrumental and stellar variability in quadrature, we can calculate the fractional uncertainty in an individual photometric data point in a manner similar to equation (36),

$$\sigma_{ind} = \sqrt{\left(\frac{\sqrt{N_S + n_{pix}(N_D + N_R^2) + N_B}}{N_S}\right)^2 + \sigma_{stel}^2} \tag{40}$$

where N_S is the number of photons collected from the source, n_{pix} is the size of the photometric aperture in pixels, N_B is the number of photons collected from the sky background, N_D is the dark current, and N_R is the read noise. The quantity σ_{stel} denotes the uncertainty from stellar variation.

To detect the transit of an Earth-like planet, we require that the transit display a S/N of at least ten. For an Earth-like planet transiting a Sun-like star, this requires a precision of 8.4 ppm. Similar to the previous calculations involving only photon counting statistics we may achieve a higher data precision by binning all of the in transit data points. This will reduce the uncertainty in an individual exposure (σ_{ind}) to

$$\sigma_{bin} = \sqrt{\frac{\sigma_{ind}^2}{n_{points}} + \sigma_{flr}^2} = \sqrt{\left(\frac{t_{exp} + t_{read}}{t_{tr}}\right)^{-1} \sigma_{ind}^2 + \sigma_{flr}^2}. \tag{41}$$

Note that we have included the noise floor from spacecraft jitter and systematics in the term σ_{flr}. Again, the exact value of the exposure time does not significantly affect the precision of the data, and so it has been fixed at 10 seconds.

To see what effect including these additional noise sources have, again consider observations of a $m_V = 6$, G2V star. As we determined in Section 3.3, photon-noise limited observations of this star require a 90.8cm^2 effective aperture to achieve a S/N=10 transit detection, and a 44.7cm^2 effective aperture for a S/N=7 detection. If we use a 10ppm noise floor from jitter and other systematics, then we see that a S/N=10 detection is no longer possible, since the required 8.4ppm precision lies below the noise floor. For S/N=7,

detections are still possible, but with a larger effective collecting area of 145.6cm^2. The third column in Table 2 displays the necessary aperture diameter for S/N=7 detections if we now include a 10ppm noise floor in the data. From equation (39), using a jitter noise of 10ppm implies that the spacecraft will have to be able to point to within 0.08pix.

For a 50ppm noise floor it becomes impossible to reach either a S/N=10 or S/N=7 detection threshold. Therefore, we instead examined what effect increasing the noise floor has on the minimum detectable planet size. Since the noise floor is relatively high, it is now the primary determinant of the data precision, and not the Poisson statistics of the collected photons. This means that the effect of a 50ppm noise floor is the same on telescopes sized for a S/N=7 detection with no noise floor, and for those sized assuming a 10ppm floor: the smallest detectable planet is increased from one Earth radius to 2.06 Earth radii. In the case of a S/N=10 detection, the minimum detectable planet size is increased to 2.45 Earth radii. The point requirement for the spacecraft is relaxed, according to equation (39), to 0.4pix.

Approaching the problem from another angle, what is the maximum allowable noise floor? We have just seen that it is possible to build a spacecraft to detect Earth-like planets with a 10ppm noise floor if we are satisfied with S/N=7 detections. As will be shown in Section 3.7 however, for detectability's sake we would like the minimum signal-to-noise of a detection to be higher; designing for a S/N=7 detection means that grazing transits - with shorter transit durations - will fall below the detection threshold. ExoPlanetSat will need to be designed to detect a central transit with a minimum of S/N=10 if it is to detect a sufficient number of grazing transits with better than S/N=7. To detect grazing transits with data stronger than S/N=10, ExoPlanetSat would need to be designed to detect central transits with a minimum S/N=14. These requirements mandate a noise floor of 8.4ppm and 6ppm, respectively, to detect an 84ppm transit. These lowered noise floors would

necessitate very stringent pointing requirements, with the spacecraft held to within 0.07pix for 8.4ppm jitter noise, and 0.05pix for 6ppm.

3.5. Focal Plane Design

The design of the focal plane for ExoPlanetSat was conducted by Dr. George Ricker. Each spacecraft will use six MIT/Lincoln Lab 512x1024 pixel CCDs. The CCDs will be set-up to operate in a frame-transfer mode with only 512x512 pixels exposed to the sky. At the end of each exposure, the 512x512 image will be quickly shifted onto the other half of the CCD, which will be covered. There the image may be read while another exposure is taking place. Shifting the image from one half of the CCD to the other will take approximately half a millisecond. Operating the CCDs in frame-transfer mode has two advantages. Firstly, the read time for each image is effectively half a millisecond, which allows for a much higher duty cycle - especially at very short exposure times. Secondly, shifting the image onto a covered portion of the CCD that quickly removes the need for a mechanical shutter in the optical system.

The choice of CCD also serves to constrain the choice of ExoPlanetSat's bandpass. Ideally, the satellite would have as wide a bandpass as possible, to collect as many photons as it can. Silicon CCDs, however, generally have quantum efficiency curves that drop to zero beyond 1000nm. On the other side of the spectrum, the CCDs available for ExoPlanetSat become ineffective at wavelengths shorter than about 400nm. At these short wavelengths, the photons cannot penetrate very far into the material of the CCD, and so have trouble exciting photo-electrons. For these reasons, ExoPlanetSat will observe between 400nm to 1000nm.

Figure 11 shows a diagram of the six CCDs assembled on the focal plane. Note

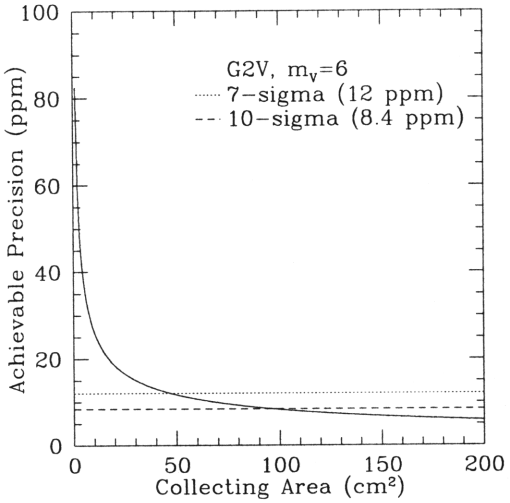

Fig. 9.— The fractional precision achievable in a single exposure of a G2 star with $m_V = 6$ as a function of the collecting area. Also shown are the 7σ and 10σ detection thresholds for detecting the transit of an Earth-like planet.

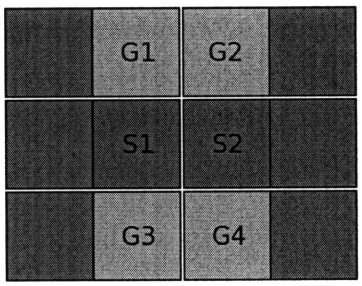

Fig. 10.— A diagram of the CCD arrangement on the ExoPlanetSat focal plane. The two science CCDs (S1 and S2) are offset 300 μm, to defocus the images. Note that all six are set-up to run in frame-transfer mode.

that only the two middle CCDs are devoted to capturing science images. The outer four detectors are connected to the spacecraft's guidance system, and will be used to take images for maintaining the pointing of the spacecraft. The guide CCDs are placed outside and separate from the science CCDs for three reasons. Firstly, tracking stars that are more widely separated on the sky improves the precision of the spacecraft's pointing. This leads to placing the guide CCDs on either side of the focal plane. Secondly, the guidance images will require exposure times that do not necessarily correspond to exposure times required for the science images. Thirdly, the science CCDs will be offset from the optical focal plane to purposefully defocus the image; using different CCDs for guidance therefore allows the spacecraft to acquire in-focus images to feed to the spacecraft's attitude control system. The two science CCDs will be deliberately defocused to even out flat-fielding errors, and to allow for longer exposure times, as discussed in the previous section on the precision requirements of the photometric data.

3.6. Designing to fit a Triple CubeSat Deployer

One scenario for ExoPlanetSat is to design the mission to fit into a triple CubeSat deployer. A CubeSat is a specific type of nanosatellite spacecraft that is 10cm on a side. Using three CubeSats stacked on top of one another (a "triple") would limit the dimensions of ExoPlanetSat to a rectangular box with sides 10cm x 10cm x 30cm. This has the immediate effect of requiring the diameter of the light collecting area be less than 10cm; with allowances for the support structure and housing, the diameter is further pushed down to 8cm.

What can be done with an 8cm telescope? As a baseline, using no noise floor or spacecraft jitter and requiring S/N=10 the dimmest stars that would show detectable transits of an Earth-sized planet would have $m_V = 5.1$. If we relax the S/N requirement

to S/N=7, then the magnitude limit increases to $m_V = 5.9$. Including a jitter noise floor of 10ppm changes the limiting magnitude for S/N=7 detections to $m_V = 4.6$. If the noise floor is engineered down to levels of 8.4ppm or 6ppm (the requirements noted at the end of Section 3.4), then this will change the limiting magnitudes to $m_V = 5.2$ for S/N=7, and $m_V = 4.4$ for S/N=10, respectively.

One way to increase the limiting magnitude of a triple CubeSat survey would be to use three spacecraft equally spaced along an orbit. If all three were targeted onto the same star, than the star could be observed continuously. This would triple the quantity t_{tr}, the time observed in transit, up to the duration of the transit itself. As noted previously, this is 13 hours for an Earth transiting a Sun-like star. Assuming a 10ppm jitter noise floor, using three spacecraft to continuously monitor a target would increase the limiting magnitude for a S/N=7 detection to $m_V = 5.8$.

The main Hipparcos catalog contains only seventy G- and K-dwarfs brighter than $m_V = 5.8$. This is unfortunately not enough stars to statistically ensure the detection of a transiting habitable-zone Earth; the *a priori* transit probability of 0.5% requires at least 200 hundred targets. Therefore, ExoPlanetSat will need to be able to detect Earth-like planets around stars fainter than the $m_V = 5.8$ limit of three triple CubeSats. This could be accomplished with a constellation of spacecraft with varying telescope sizes, with the larger spacecraft assigned to the dimmer stars.

3.7. The Effect of Non-central Transits

In the preceding sections we made the implicit assumption that ExoPlanetSat was observing central transits across the parent star. It is worth considering the effect of non-central transits on a planet's detectability. In Section 3.3, we determined that since

ExoPlanetSat will bin all of the in transit data, that the precision of the photometry is given by equation (37). By extension, the S/N of a transit is

$$S/N = \sqrt{\frac{t_{tr}}{t_{exp} + t_{read}}} \frac{\delta}{\sigma_{ind}}, \tag{42}$$

where δ is the depth of the transit. Note that the S/N of a transit is proportional to the square root of the transit duration; grazing transits reduce the transit duration by a factor of $\sqrt{1 - b^2}$ - where b is the impact parameter of the transit. We may relate this reduction in signal-to-noise to the S/N of a central transit as

$$S/N = S/N_{cen}(1 - b^2)^{1/4}. \tag{43}$$

Now, consider that the ExoPlanet Survey will have a minimum S/N requirement for detections. For a given S/N of a central transit, this implies that grazing transits in the same star may be detected up to a maximum impact parameter of

$$b_{max} = \sqrt{1 - \left(\frac{S/N_{min}}{S/N_{cen}}\right)^4}. \tag{44}$$

The detection probability for a planetary transit is the probability that the impact parameter of a transit will be less than this b_{max}. This is distinct from the transit probability, which is the probability that the impact parameter will be between zero and one. Using stellar orientation measurements, the detection probability can be calculated by integrating equation (12) from zero to b_{max}. For the assumptions we have made for the design of the survey - a stellar orientation of $I = 90° \pm 2.5°$ and planetary inclinations uniformly distributed within $\pm 5°$ - the distribution of $f_B(b)$ is effectively flat between the values of $b = 0$ and $b = 1$: the difference is 0.13%. With very little loss of accuracy we may therefore say that the detection probability is directly proportional to the value of b_{max}.

The effect of this is to decrease the chance that a planetary system is detected. For example, if ExoPlanetSat has a jitter-induced noise floor of 10ppm and a requirement of

S/N=7 for detection, then at best one could detect 72% of all transiting Earths, since the noise floor imposes a maximum S/N for central transits of 8.4. Coupled with a transit probability of 5%, this would mean that the chances of spotting a habitable-zone Earth transiting the target star would be 3.6%. In determining the number of spacecraft and the size of the telescopes required for the ExoPlanetSat constellation, this decrease in the detectability due to non-central transits can either be accepted, or the noise floor in the data from jitter and other systematics can be reduced. Creating larger telescopes is another option, and would help to improve the photon statistics, but this would only be a marginal gain, since the noise floor sets a hard limit on the maximum value of S/N_{cen}.

4. Concept of Operations

To enable observations of all the desired target stars, the ExoPlanetSat constellation will be composed of multiple satellites with varying telescope sizes. The individually targeted spacecraft are a sharp contrast to other photometric transit surveys, which observe all the stars within a given field. As noted before, however, the brightness of the ExoPlanetSat targets requires that each star be observed individually, since the stars are too distant from one another on the sky to fall into the same field of view. In turn, the selection of these specific target stars gives us the opportunity to custom size each of the ExoPlanetSat spacecraft.

The target stars for ExoPlanetSat will first be identified on the ground. Measurements of the stellar orientation, either using spectroscopic $v \sin(I)$ or asteroseismology, and selection of those stars with orientations near 90°, will provide the initial cut to determine viable transit targets. The asteroseismologic observations will require approximately 6 months per star (T. Campante, private communication). The radial velocity data obtained for the asteroseismology can also be used to determine if the target stars are in multiple star

systems. This pre-selection of the ExoPlanetSat target stars will allow the constellation to take advantage of the stellar orientation measurements, and also will help remove the most common types of false positives.

The magnitude range that the ExoPlanet Sat spacecraft will have to cover was discussed briefly in Section 3 as $0 \leq m_V \leq 7$. This range is motivated by the requirement for three detections of habitable-zone Earths. Assuming that every star has an Earth in a habitable-zone orbit, the sample size must be at least 680 stars for there to be a 50% chance that there are more than three transiting habitable-zone Earths in the sample. The sample size is calculated by integrating the binomial distribution and solving the equation

$$0.5 = \int_3^\infty \left(\begin{array}{c} n \\ 3 \end{array} \right) \left(\frac{1}{215} \right)^3 \left(1 - \frac{1}{215} \right)^{n-3} ds. \tag{45}$$

for n, the number of trials. Note that we have used the *a priori* transit probability for habitable-zone planets of $R_*/a = 1/215$ as the probability of success.

For our initial design purposes, we used the main Hipparcos catalog (Perryman et al. 1997) to make a rough estimate of what limiting V-magnitude was needed to satisfy the requirement for 680 stars. A limit of $m_V = 7$ gave approximately 775 G- and K-dwarfs — though a more detailed accounting is currently underway, since some of these stars may be in binaries or too variable to allow a transit detection. We therefore note that a limiting magnitude of $m_V = 7$ is only a first approximation. Additionally, we have made the assumption that every star has an Earth-like planet in its habitable-zone. While this is probably not the case, in the absence of any concrete statistics for Earth-sized worlds around solar-type stars we consider it to be conceptually the most straightforward assumption.

Even though the sample size for ExoPlanet Sat must be greater than 680 stars, this is neither the number of stars that will be observed, nor is it the number of spacecraft that will have to be launched. The number of stars that ExoPlanet Sat will have to

observe will instead be determined by the the survey's window function, the detectable fraction of non-central transits, and the transit probability given through stellar orientation measurements. The window probability - or function - of a photometric survey describes the probability that the survey will be able to detect signals with a given period. It is determined by how long, and how often, the target is observed. Most ground-based surveys have window functions that remain near unity until about ten days, and then fall away for longer periods. Since the ground-based surveys always observe at the same time of day (i.e. - night) they are also afflicted with aliasing at integer and half-integer day long periods, since a hypothetical signal with a period of exactly a day would either be "on" and always occurring when the survey was looking, or "off" and never occurring.

ExoPlanetSat will also have a window probability, but it will be determined by the orbit of the spacecraft. Instead of a twenty-four hour day and eight hour night, ExoPlanetSat will have a ninety minute day and thirty-eight minute night. This is short enough that aliasing will not be an issue for ExoPlanetSat. A habitable-zone Earth would take 13 hours to transit a star the size of the Sun; this long transit duration relative to the orbital period of the spacecraft means that ExoPlanetSat will always capture a portion of the transit. Therefore, assuming that an ExoPlanetSat spacecraft is able to observe a target star for at least two years (the minimum to detect two transits), the window probability for the survey will be unity.

The transit probability for a habitable-zone Earth around a solar-like star, which we take to imply an orbital radius ratio of $R_*/a = 1/215$, can be calculated for various orientation measurements of the form $I \pm \sigma$ by using equation (28) to account for the inclination of the planetary system:

$$P_{tr}(I) = \int_{90°-.2665°}^{90°+.2665°} \int_{0°}^{180°} \left(\frac{1}{\sigma\sqrt{2\pi}} \exp\left[\frac{-(\psi - I)^2}{2\sigma^2} \right] \right) \left(\frac{H(i - \psi + 5°)H(-i + \psi + 5°)}{2\sigma} \right) d\psi \, di. \tag{46}$$

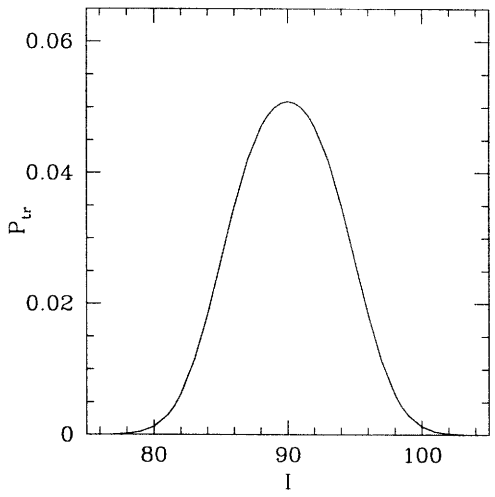

Fig. 11.— The transit probability P_{tr}, including the effects of planetary inclinations, as a function of the measured stellar inclination angle $I \pm 2.5°$.

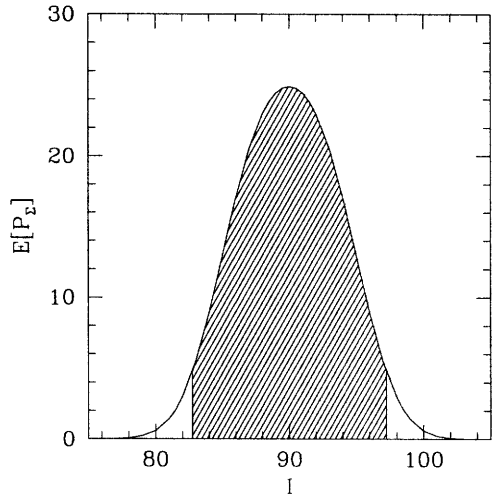

Fig. 12.— The expected transit probability $E[P_\Sigma(I)]$. as a function of the measured stellar inclination angle $I \pm 2.5°$. The shaded region covers 95% of the distribution.

Figure 12 shows P_{tr} for a range of inclinations I assuming asteroseismic measurements of the orientation with $\sigma = 2.5°$. The overall transit probability will be this function multiplied by the window probability and the detectable fraction of non-central transits which we determined in Section 3.7:

$$P_{\Sigma}(I) = P_{win}\ P_{det}\ P_{tr}(I). \tag{47}$$

To find the number of stars that ExoPlanet Sat will have to observe, we begin by multiplying $P_{\Sigma}(I)$ by the probability that a star will show a measurement of I. This will give the expected average value of $P_{\Sigma}(I)$. Since the 680 stars within our sample are randomly oriented, the probability that measuring a certain star yields a stellar inclination angle of I goes as $\sin(I)$. Scaling this to the size of our sample, the expected value of $P_{\Sigma}(I)$ will be

$$E[P_{\Sigma}(I)] = 680\ \sin(I)\ P_{\Sigma}(I). \tag{48}$$

Since the sine function is close to flat near 90°, the functional form of equation (49) is very close to that of $P_{\Sigma}(I)$ (Figure 13). We will require that ExoPlanetSat is able to detect 95% of all the transiting planets within our 680 star sample. This corresponds observing stars over a range of inclinations sufficient to encompass 95% of the distribution of $E[P_{\Sigma}(I)]$. We therefore solve

$$0.95 = \frac{\int_{90-\phi}^{90} \sin(I)\ P_{\Sigma}(I)}{\int_{0}^{90} \sin(I)\ P_{\Sigma}(I)}. \tag{49}$$

Doing so numerically, we find that $\phi = 7.25°$. That is to say, ExoPlanetSat will have to observe all of the stars with measured inclinations within the range $82.75° \leq I \leq 90°$ if it is to find 95% of the transiting planets within the sample of 680 stars. Since the stars within the sample are randomly oriented, this will mean that ExoPlanetSat will need to observe

$$680\ \cos(82.75°) = 86 \tag{50}$$

target stars to have a high confidence of detecting three transiting Earths in the habitable-zone.

To figure the number of spacecraft needed to observe 86 targets, consider the simplest case of one spacecraft for each star. As calculated in Section 3.4, for a 10ppm noise floor, an average magnitude limit of $m_V = 6$, and requiring S/N=7, having one spacecraft per star will require telescopes with an average diameter of 15.1cm.

Note, however, that having one spacecraft per star does not necessarily imply that 86 spacecraft need to be built. If the spacecraft are built to have a reasonable on orbit lifetime of four to five years, then much less than 86 spacecraft are required. Consider, for example, a constellation of thirty spacecraft that are each assigned one to a star. Statistically speaking, after one year of observing only one of the stars should show a transit. This allows for the other twenty nine spacecraft to be re-targeted onto other stars for the second year of observing, and similarly for the third year, after which all of the target stars will have been observed. Allowing for an additional year's worth of observation time to secure a second transit on the last identified system, 30 spacecraft could survey all 86 stars within four years. Therefore, the real determinant of how many spacecraft are needed is the orbital lifetime of ExoPlanetSat. We will assume that the spacecraft can stay in orbit and collect observations for four years.

What happens if we change the number of spacecraft targeted at each star? If we instead task each spacecraft with observing two stars, then the total amount of time that each transit can be observed is cut in half, and drops from 4.3 hours to 2.15 hours. For the same limiting magnitude, this would mean that the size of each of the telescopes on the spacecraft would need to increase to achieve the same S/N. Similarly, increasing the number of telescopes targeted at each star to two per star or to three per star decreases the size of the telescopes for the same limiting magnitude. Table 3 shows the number of spacecraft and telescope sizes needed in these cases, assuming a fixed limiting magnitude. Alternately, we may keep the size of the telescopes the same but allow the magnitude limit

to vary depending upon how many spacecraft are targeted at each star. Table 4 shows how the limit shifts in these different scenarios.

In Section 3.6 we described the limits of an ExoPlanetSat built to fit a triple CubeSat deployer. This would limit each ExoPlanetSat spacecraft to a telescope 8cm in diameter, and using one spacecraft per star with a noise floor of 10ppm places the magnitude limit at $m_V = 4.6$ for a S/N=7 detection. Shifting to three spacecraft per star increases the limiting magnitude to $m_V = 5.8$, and going even further, to six spacecraft per star, places the magnitude limit at $m_V = 6.6$. If we again consider 30 spacecraft in orbit, six spacecraft per star would allow a triple CubeSat based constellation to survey twenty to twenty five stars within a four to five year orbital lifetime. This would only partially complete the survey of the 86 target stars, but one would observe enough stars to have one expected detection of a habitable-zone Earth. Nevertheless, triple CubeSat sized spacecraft should be partnered with spacecraft that have larger telescopes to more efficiently survey the dimmer target stars.

To determine what such a partnering would look like, consider the Hipparcos star counts for G- and K-dwarfs in Table 5. By proportionally distributing the 86 target stars across the four magnitude bins, we can make a rough estimate for how many of the 86 target stars will lay in which magnitude ranges. Now, if we assign six triple CubeSat sized spacecraft onto each target star brighter than $m_V = 5$ we will have to observe approximately seven targets; over four years this can be done with 9 spacecraft split into three trios. For the stars in the magnitude range $5 \leq m_v \leq 6$, ExoPlanetSat will need to observe 19 stars. Using one 15.1cm diameter telescope per star, all 19 stars stars can be surveyed with seven spacecraft over four years. Finally, the approximately 60 faintest stars between $6 \leq m_v \leq 7$ can be observed by targeting three 15.1cm diameter telescopes onto each star. To cover all 60 targets in four years, this will require 45 spacecraft, organized into fifteen groups

of three. In total, surveying the 86 target stars in this way will require 9 triple CubeSat spacecraft and 52 spacecraft with 15.1cm diameter telescopes.

5. Conclusion

With the drive towards finding Earth-sized extrasolar planets — particularly habitable-zone ones — it is becoming necessary to conduct photometric transit surveys from space. Unfortunately, the large angular separation between the brightest stars in the sky means that all of the currently proposed and operating space-based surveys ignore these targets. Here, we have examined a survey designed to probe the brightest solar-like stars for habitable-zone Earth-sized planets.

By using measurements of the orientation of the stellar rotation axis obtained through spectroscopic measurement of $v \sin(I)$, or more precisely through asteroseismology, we are able to increase the transit probability of a habitable-zone Earth by an order of magnitude from 0.5% to 5%. Even factoring in the fraction of non-central transits that we expect to be not detectable, the probability of seeing a detectable transit for a star with an asteroseismologically determined orientation is 3.6%. This increase means that instead of having to observe 600 hundred stars to expect three detections of an habitable-zone Earths, ExoPlanetSat will only have to observe 86. This enables the design of a practical survey that can be accomplished with a reasonable amount of hardware within a reasonable amount of time.

We have considered many different scenarios for the design of the survey, varying the expected noise floor, the desired magnitude limit for detections, and the number of spacecraft targeted at each star. The baseline survey that we have imagined consists of thirty spacecraft with 15.1cm diameter telescopes, each targeting their own individual star.

With a photometric noise floor of 10ppm and a magnitude limit of $m_V = 6$, these spacecraft could complete the survey within four years.

Another possibility is to use satellites sized to fit into a triple CubeSat deployer. This limits the telescope diameter to 8cm, and with three spacecraft on a star the magnitude limit for the survey would be $m_V = 5.8$ for a 10ppm noise floor. If the number of spacecraft targeted at each star is increased to six, then the magnitude limit increases to $m_V = 6.6$. This is enough to conduct a partial survey of twenty to twenty-five stars over the course of four to five years, but serves to illustrate the utility of partnering triple CubeSat sized satellites with larger spacecraft that can more efficiently survey the dimmer target stars.

Whatever the exact makeup of the ExoPlanetSat constellation, their is a need for a photometric survey of the brightest stars in the sky if only because the scientific payoff of an Earth orbiting in the habitable-zone of one of the brightest stars would be enormous. A bright host star makes spectroscopic determination of the planetary mass practical. This is in contrast to other space-based surveys such as Kepler, which target dim stars that are challenging radial velocity targets.

Additionally, an Earth-like planet around a bright star is a prime candidate for follow-on work using future instruments such as JWST. Successfully detecting a transmission spectrum of the planetary atmosphere, measuring the out-of-eclipse photometric variation, or any other observational objective becomes much more feasible for a planet around a bright host star. It may be even possible, if a planet is found around one of the brightest - and nearest - stars to obtain an astrometric (or even direct imaging) detection. While ExoPlanetSat will not conduct these sorts of observations, the survey does offer a jumping-off point as the means to identify these promising systems around the brightest stars.

REFERENCES

Aigrain, S., et al. 2009, arXiv:0903.1829

Aldering, G. 2001, LBNL report number LBNL-51157

Alonso, R., et al. 2004, ApJ, 613, L153

Arentoft, T., et al. 2008, ApJ, 687, 1180

Bakos, G., Noyes, R. W., Kovács, G., Stanek, K. Z., Sasselov, D. D., & Domsa, I. 2004, PASP, 116, 266

Ballot, J., Appourchaux, T., Toutain, T., & Guittet, M. 2008, A&A, 486, 86

Bazot, M., Bouchy, F., Kjeldsen, H., Charpinet, S., Laymand, M., & Vauclair, S. 2007, A&A, 470, 295

Beatty, T. G., & Gaudi, B. S. 2008, ApJ, 686, 1302

Beck, J. G., & Giles, P. 2005, ApJ, 621, L153

Bedding, T. R., & Kjeldsen, H. 2008, 14th Cambridge Workshop on Cool Stars, Stellar Systems, and the Sun, 384, 21

Borucki, W. J., & Summers, A. L. 1984, Icarus, 58, 121

Charbonneau, D., Brown, T. M., Latham, D. W., & Mayor, M. 2000, ApJ, 529, L45

Cox, A. N. 2000, Allen's Astrophysical Quantities, 4th ed. New York: AIP Press.

Fabrycky, D. C., & Winn, J. N. 2009, arXiv:0902.0737

Gizon, L., & Solanki, S. K. 2003, ApJ, 589, 1009

Henry, G. W., Marcy, G. W., Butler, R. P., & Vogt, S. S. 2000, ApJ, 529, L41

Koch, D. G., Borucki, W. J., Dunham, E. W., Jenkins, J. M., Webster, L., & Witteborn, F. 2000, Proc. SPIE, 4013, 508

Kurucz, R. L. 1979, ApJS, 40, 1

Ledoux, P. 1951, ApJ, 114, 373

Martić, M., et al. 1999, A&A, 351, 993

McCullough, P. R., Stys, J. E., Valenti, J. A., Fleming, S. W., Janes, K. A., & Heasley, J. N. 2005, PASP, 117, 783

Nutzman, P., & Charbonneau, D. 2008, PASP, 120, 31

Ohta, Y., Taruya, A., & Suto, Y. 2005, ApJ, 622, 1118

Perryman, M. A. C., et al. 1997, A&A, 323, L49

Reegen, P., et al. 2006, MNRAS, 367, 1417

Southworth, J., et al. 2009, arXiv:0903.2139

Street, R. A., et al. 2003, Scientific Frontiers in Research on Extrasolar Planets, 294, 405

Winn, J. N., et al. 2006, ApJ, 653, L69

Winn, J. N., et al. 2007, AJ, 133, 1828

Yi, S., Demarque, P., Kim, Y.-C., Lee, Y.-W., Ree, C. H., Lejeune, T., & Barnes, S. 2001, ApJS, 136, 417

This manuscript was prepared with the AAS LaTeX macros v5.2.

Table 1. PHOTON COUNTS ($m_V = 6$)

Spec. Type	T_{eff} (K)	Counts (γ s^{-1} cm^{-2})
G0	6000	10,669
G2	5750	10,162
G6	5500	11,393
G9	5250	11,867
K2	4750	13,067
K4	4500	14,360
K6	4250	15,703
K7	4000	17,032

Table 2. REQUIRED APERTURE DIAMETER

Magnitude Range	σ_{flr} = 0ppm S/N=10	σ_{flr} = 0ppm S/N=7	σ_{flr} = 10ppm S/N=7
$0 \leq m_v \leq 4$	4.8cm	3.3cm	6.0cm
$4 \leq m_v \leq 5$	7.5cm	5.3cm	9.5cm
$5 \leq m_v \leq 6$	11.9cm	8.4cm	15.1cm
$6 \leq m_v \leq 7$	18.9cm	13.3cm	24.0cm

Table 3. COMPARISON OF SURVEY SCENARIOS (FIXED MAG. LIMIT)

Tel. per Star	No. Spacecraft	Size (cm)	Limiting Magnitude
0.5	15	21.4	6.0
1	30	15.1	6.0
2	60	10.7	6.0
3	90	8.7	6.0

Table 4. COMPARISON OF SURVEY SCENARIOS (FIXED AREA)

Tel. per Star	No. Spacecraft	Size (cm)	Limiting Magnitude
0.5	15	15.1	5.2
1	30	15.1	6.0
2	60	15.1	6.8
3	90	15.1	7.2

Table 5. EXPECTED TARGET STAR DISTRIBUTION

Mag. Range	G/K Dwarfs (%)	Target Stars
$0 \leq m_v \leq 4$	22 (3%)	2
$4 \leq m_v \leq 5$	43 (5.5%)	5
$5 \leq m_v \leq 6$	171 (22%)	19
$6 \leq m_v \leq 7$	39 (69.5%)	60
Total	775 (100%)	86